Micromagnetic study of excitation modes of an artificial skyrmion crystal

Cite as: Appl. Phys. Lett. **107**, 222402 (2015); https://doi.org/10.1063/1.4936756
Submitted: 30 September 2015 . Accepted: 14 November 2015 . Published Online: 30 November 2015

B. F. Miao, Y. Wen, M. Yan, L. Sun, R. X. Cao, D. Wu, B. You, Z. S. Jiang, and H. F. Ding

Micromagnetic study of excitation modes of an artificial skyrmion crystal

B. F. Miao,[1] Y. Wen,[1] M. Yan,[2] L. Sun,[1,3] R. X. Cao,[1] D. Wu,[1,3] B. You,[1,3] Z. S. Jiang,[1] and H. F. Ding[1,3,a)]

[1]*Department of Physics, National Laboratory of Solid State Microstructures, Nanjing University, 22 Hankou Road, Nanjing 210093, People's Republic of China*

[2]*Department of Physics, Shanghai University, 99 Shangda Road, Shanghai 200444, People's Republic of China*

[3]*Collaborative Innovation Center of Advanced Microstructures, Nanjing University, 22 Hankou Road, Nanjing 210093, People's Republic of China*

(Received 30 September 2015; accepted 14 November 2015; published online 30 November 2015)

We present a micromagnetic study on the eigen excitations of an artificial skyrmion crystal, which has been experimentally confirmed to be stable at room temperature without the need of any Dzyaloshinsky-Moriya interaction (DMI). Three in-plane rotational modes and one breathing-type mode are identified. We find the intrinsic origin of the dynamics of skyrmion crystal is the nontrivial magnetic texture instead of DMI. And the rotational direction of a skyrmion is solely determined by the sign of the skyrmion number, irrespective of its circulation sense, evidencing the topological nature of the magnetic skyrmion. © *2015 AIP Publishing LLC*.
[http://dx.doi.org/10.1063/1.4936756]

A magnetic skyrmion is a topological object with a swirling spin structure, which carries topological charge and Berry phase in real space. After the reciprocal- and real-space observations in B20 materials, such as MnSi and FeCoSi, by neutron diffraction and Lorentz transmission electron microscopy,[1,2] the magnetic skyrmion has attracted considerable attention due to its fundamental interests and great potential for application.[3–12] Typically, the formation of skyrmion crystal requires the presence of Dzyaloshinsky-Moriya interaction (DMI) and was found to be stable only within a narrow temperature-magnetic field region,[1,13,14] which impedes its physical exploration and application greatly. Although the situation improves in thin films[12,15,16] and DMI induced room temperature skyrmion crystal was also reported very recently,[17–19] its reliance on the DMI strongly limits the material selection of Skyrmion crystals. To overcome/bypass these obstacles, Sun *et al*. and Dai *et al*. proposed an approach to create artificial skyrmion crystal with ordinary magnetic material through the dipolar-dipolar interaction.[20,21] By embedding a magnetic vortex state into an out-of-plane magnetized environment, such artificial skyrmion crystal have been realized experimentally at room-temperature.[22–24] Without the limitation of DMI, artificial skyrmion crystal significantly expands the pool of prospective materials in the future skyrmion-based application devices.

A skyrmion crystal can exhibit many unconventional phenomena, including the topological Hall effect,[5,25] specific heat anomaly,[26] and be driven by a charge or spin current of ultralow density.[3,4] Mochizuki first theoretically investigated the spin-wave excitations in insulating skyrmion lattice with DMI.[27] It was found that the skyrmion lattice has two in-plane rotational modes and one out-of-plane breathing-type mode, which are referred as counterclockwise (CCW) mode, clockwise (CW) mode, and breathing mode, respectively.[27] Later on, the dynamics of skyrmion crystal have been studied experimentally.[28–30] On the other hand, the dynamic properties of artificial skyrmion crystal were seldom addressed. The understanding of dynamics of artificial skyrmion is an important issue for its application in the future besides the fundamental interest. In particular, the topological number of an artificial skyrmion is found to be tunable with external triggers, which provides additional parameters to control its property.[20,22,23] Meanwhile, it is also interesting to identify the intrinsic origin of the dynamics of skyrmion crystal, either from DMI or nontrivial magnetic texture. In this work, we present the micromagnetic study of the excitation spectrum of an experimentally confirmed artificial skyrmion crystal.[22–24] In the case of positive skyrmion number ($S = 1$), two CCW modes, one CW mode, and one breathing mode were identified in our simulations, resembling the results in a DMI induced skyrmion crystal. This similarity suggests that topological structure rather than DMI is intrinsically responsible for the dynamics of skyrmion crystal. Furthermore, we find that the sign of skyrmion number has great influence on its dynamic behavior.

We study the excitation modes of a two-dimensional (2D) artificial skyrmion crystal using the NIST OOMMF code.[31] Co with zero crystalline anisotropy is chosen as the disk material. And for the perpendicular magnetic film, CoPt with the uniaxial perpendicular anisotropy $K_1^{\mathrm{CoPt}} = 4.0 \times 10^5 \mathrm{J/m^3}$ is used.[32] The material parameters used in the calculations are exchange constant: $A = 1.9 \times 10^{-11} \mathrm{J/m}$; saturation magnetization: $M_s^{\mathrm{Co}} = 1.4 \times 10^6 \mathrm{A/m}$ for Co;[14] and $M_s^{\mathrm{CoPt}} = 5.0 \times 10^5 \mathrm{A/m}$ for CoPt.[32,33] The thickness of the Co disk and the CoPt perpendicular film is 24 nm and 8 nm, respectively. The Co disk diameter is D = 90 nm, with a center-to-center distance 100 nm. In the calculations, we apply 2D periodical boundary conditions within the plane and a grid size of $2 \times 2 \times 2\,\mathrm{nm^3}$. The Gilbert damping constant α is set to 0.02 in all the calculations.

a)Author to whom correspondence should be addressed. Electronic mail: hfding@nju.edu.cn

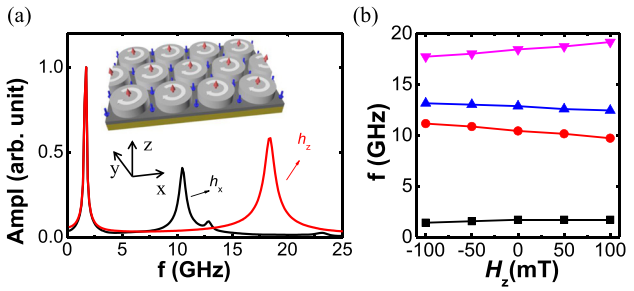

FIG. 1. (a) Magnetic excitation spectrum for a skyrmion crystal with skyrmion number $S = 1$ under in-plane (black curve) and out-of-plane (red curve) excitation. The inset shows the schematic of a 2D artificial skyrmion crystal. Ordered arrays of vortex disks are prepared on top of a film with perpendicular anisotropy. The arrows represent the orientation of the local magnetization. (b) Dependence of the four resonant frequencies on the dc perpendicular magnetic field H_z.

The inset of Fig. 1(a) presents the schematics of our created artificial skyrmion crystal, where the disk arrays are implanted into films with perpendicular magnetization. With proper selection of the aspect ratio between the diameter and thickness, the disks can be configured into a vortex state.[34,35] In this specific structure, the area in between vortex arrays will form a distorted anti-vortex. For a vortex with positive polarity, the spin swirls around the upper hemisphere and has a skyrmion number $S = 1/2$.[36,37] Meanwhile, a central negatively magnetized anti-vortex also has a skyrmion number $S = 1/2$, with spin pointing to all possible direction in the lower hemisphere.[36,37] Thus, the spin direction wraps into a sphere within one unit cell, resulting in a skyrmion number $S = 1$. In this way, an artificial skyrmion crystal can be formed, which has been experimentally realized recently.[22–24] With proper field operation sequence, skyrmion number S can be switched among 1, −1, or 0, and these states can be stable even at zero field.[22]

In order to excite resonance modes in the skyrmion state ($S = 1$) at zero static field, we apply a Gaussian shaped pulse field with an amplitude $h_0 = 10$ mT and width $w = 20$ ps along x-direction/z-direction, respectively. After this perturbation, the time evolution of the magnetization of each cell is calculated. Fourier transform is then performed on the time evolution of the out-of-plane component of magnetization (m_z) in each cell, which yields the amplitude A_i and phase ϕ_i of each cell as a function of frequency. The frequency resolution in our study is $1/(T_{\text{end}} - T_{\text{start}}) = 1/7$ ns $= 0.14$ GHz. The Fourier spectrum usually consists of a certain number of sharp peaks. Each of them indicates a resolved eigen-mode of the system.[27,38,39] By plotting the real part of the Fourier transform $A_i \cos\phi_i$ at a certain resonance frequency determined from the spectrum, we can reconstruct the spatial profile of the corresponding eigenmode, where $A_i \cos\phi_i$ represents a snapshot of the dynamical out-of-plane component of the magnetization m_z at the specific frequency.[40–42] In Fig. 1(a), we show the calculated spectra for the skyrmion state ($S = 1$) excited by in-plane (black curve) and out-of-plane (red curve) Gaussian shaped pulse field, respectively. The data have been normalized by the maximum value of each curve. Three resonance peaks can be observed under in-plane pulse field, located at 1.72 GHz, 10.44 GHz, and 12.88 GHz, respectively, while the out-of-plane pulse perturbation only yields two peaks at 1.72 GHz and 18.45 GHz, respectively. As will also be discussed in the following part, the highest frequency peak at 18.45 GHz is an out-of-plane mode which can only be excited by an out-of-plane field. And due to the fact that OOMMF uses rectangular mesh to construct the Co disks, the circular symmetry of each Co disk near the edge is inevitably broken. Thus, the out-of-plane distortion of the magnetization also disturbs the in-plane component, causing the excitations of the in-plane modes at 1.72 GHz as well. Fig. 1(b) presents the evolution of four characteristic frequencies under different dc perpendicular fields, H_z. The lowest mode has a weak field dependence and its resonance frequency increases slowly with H_z. Both two medium modes are red-shifted as H_z increases, while the highest one is blue-shifted.

To identify each resonance mode, we present the snapshot of dynamical m_z [Fig. 2(a) left column] and phase ϕ_i [Fig. 2(a) right column] for each of the four eigen-modes of the artificial skyrmion. In the scale bar of m_z, red (blue) represents the positive (negative) absolute value of maximum. In the scale bar of ϕ, red, green, and yellow represents $-\pi/2$, $\pi/2$, $\pm\pi$ for the phase, respectively. Since for each mode, every individual skyrmion in the crystal behaves the same way, we focus on only one skyrmion unit hereafter. In Fig. 2(a) showing the first mode, m_z has both a blue and a red spots separated by two azimuthal nodes, which would rotate around the center as a function of time. The phase changes from $-\pi$ to π in the CCW sense. This mode is the strongest and with lowest-frequency, which corresponds to the gyration mode of a magnetic vortex core.[43,44] The dynamic m_z at 10.44 GHz and 12.88 GHz shows similar features as that at 1.72 GHz, while the phase winds in the sense of CW and CCW, respectively. The two medium frequency modes correspond to the CW and CCW rotational mode of skyrmion crystal, respectively. And we will further clarify this point by applying oscillating field at given frequencies in the following discussion. For the highest frequency mode at h_z pulse perturbation, the dynamic m_z exhibits ring pattern with concentric nodes only in the center of the disk and at its border, and the phase is almost uniform over the skyrmion [Fig. 2(a) for the 4th mode]. This mode corresponds to the breathing mode of skyrmion crystal.

We further study the spin dynamics by applying a continuous oscillating magnetic field at the resonant frequency f_r to the skyrmion crystal with skyrmion number $S = 1$. First, an *in-plane* ac magnetic field is applied to the crystal to activate in-plane resonant modes, which is set as $\boldsymbol{h}(t) = (h_x^f \sin(2\pi f t), 0, 0)$, with $h_x^f = 10$ mT. Figures 3(a)–3(c) demonstrate the time evolutions of the magnetization for the skyrmion state ($S = 1$) under a 1.72 GHz, 10.44 GHz, and 12.88 GHz ac in-plane field, respectively. In the magnetic configuration, the red/blue color denotes the magnetization component coming out-of-/into-surface, while the black arrow represents the in-plane direction. We find that the skyrmion core rotates in the sense of CCW for the low-lying mode, CW for the medium-mode, and CCW for the higher in-plane mode. The directions of their rotation are consistent with the phase profile calculated from Fourier Transformation in Fig. 2(a). Equally interesting, the rotation directions are independent of the winding direction of spins in

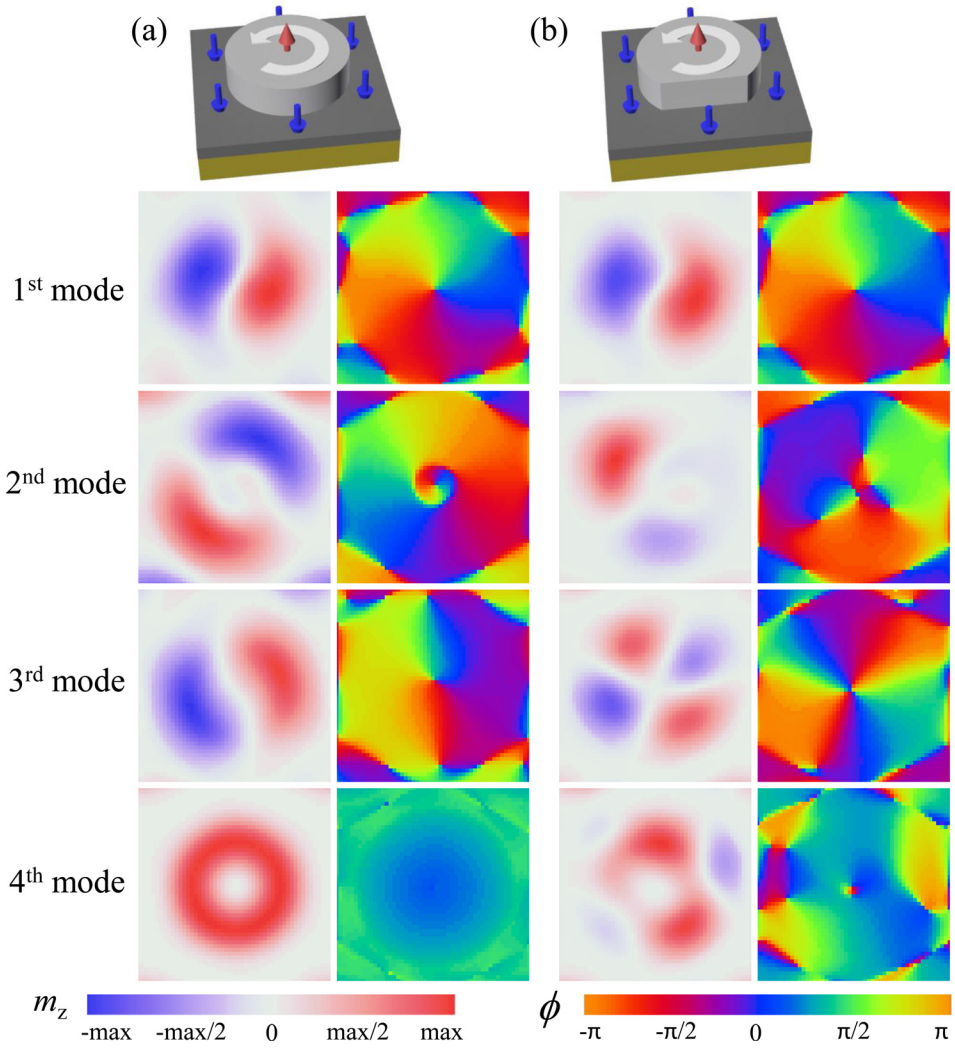

FIG. 2. (a) Snapshots of the dynamic m_z (left column) and phase ϕ (right column) at different eigen frequencies for a skyrmion state with $S=1$. The 1st, 2nd, and 3rd are azimuthal-like modes, and 4th is a radial-like mode. (b) For comparison, we also present the results for a skyrmion crystal consisting of edge-cut Co disks. The color bars on the bottom are applicable for both (a) and (b).

the skyrmion [Fig. 3(d)]. Instead, they are determined by the skyrmion number, manifesting its topologic nature of the dynamic behavior. For instance, the skyrmion of a skyrmion crystal with $S=-1$ [Fig. 3(e)] rotates in the sense of CCW at 10.44 GHz, opposite to the skyrmion with $S=1$ [Figs. 3(b) and 3(d)]. Under the *out-of-plane* ac field at 18.45 GHz, the skyrmion oscillates in the breathing mode, with its core extends and shrinks periodically with time [Fig. 4(a)]. Similar to the in-plane rotational modes, the skyrmion state with opposite skyrmion number breathes out-of-phase with each other [Fig. 4(b)].

We also calculated the dynamics of an isolated skyrmion and found it has similar features for skyrmion crystal as discussed above. In addition, we calculated the dynamics behavior of skyrmion crystal with Co disk in the edge-cut geometry. Due to the fact that skyrmion is a topologically protected object, it is inertial under small perturbation. Thus, the skyrmion crystal with edge-cutting Co disk and circular Co disk exhibit similar dynamic feature, three in-plane rotational modes and one out-of-plane breathing mode are observed [Fig. 2(b)]. And in the two cases, the skyrmion crystal gyrates in the same way for the low-lying three in-plane modes. Due to the breaking of the circular symmetry of the Co disk with an edge-cut shape, the spatial distributions of m_z and ϕ are distorted compared to those of a circular Co disk, especially at higher frequencies. For instance, the blue spot in dynamic m_z of the 2nd mode is very light, and m_z exhibits a distorted ring pattern in the highest frequency mode; and the phase ϕ also changes accordingly. In the 3rd mode, we observe two red spots located at the upper-left and the lower-right part, and two blue spots at the upper-right and lower-left part. This is mainly caused by the stronger interaction of in-plane and out-of-plane resonance as the circular symmetry is broken in the edge-cut disk.

Finally, we compare the spin-wave modes calculated herein for an artificial skyrmion with those of the skyrmion arising from the DMI, which were recently reported in Ref. 27. In the previous study, it was found that two rotational modes exist under an in-plane ac field, with a CCW (CW) fashion for the lower-lying (higher-lying) mode. And out-of-plane ac field can excite the breathing mode. It is important to note that the skyrmion number $S=-1$ in Ref. 27 with the core pointing down and the periphery part pointing up. So, the positive direction of the magnetic field H_z is opposite to our definition here. As already demonstrated in Fig. 3, the directions of rotation modes of skyrmion crystal with $S=1$ are opposite with that of $S=-1$. As a result, the CCW mode, CW mode, and breathing mode in Ref. 27 corresponds to the CW mode (10.44 GHz), CCW mode (12.88 GHz) and breathing mode (18.45 GHz) in this work. Therefore, all these modes in artificial skyrmion have the same field dependence with those in skyrmion of DMI [Fig. 1(b)]. The

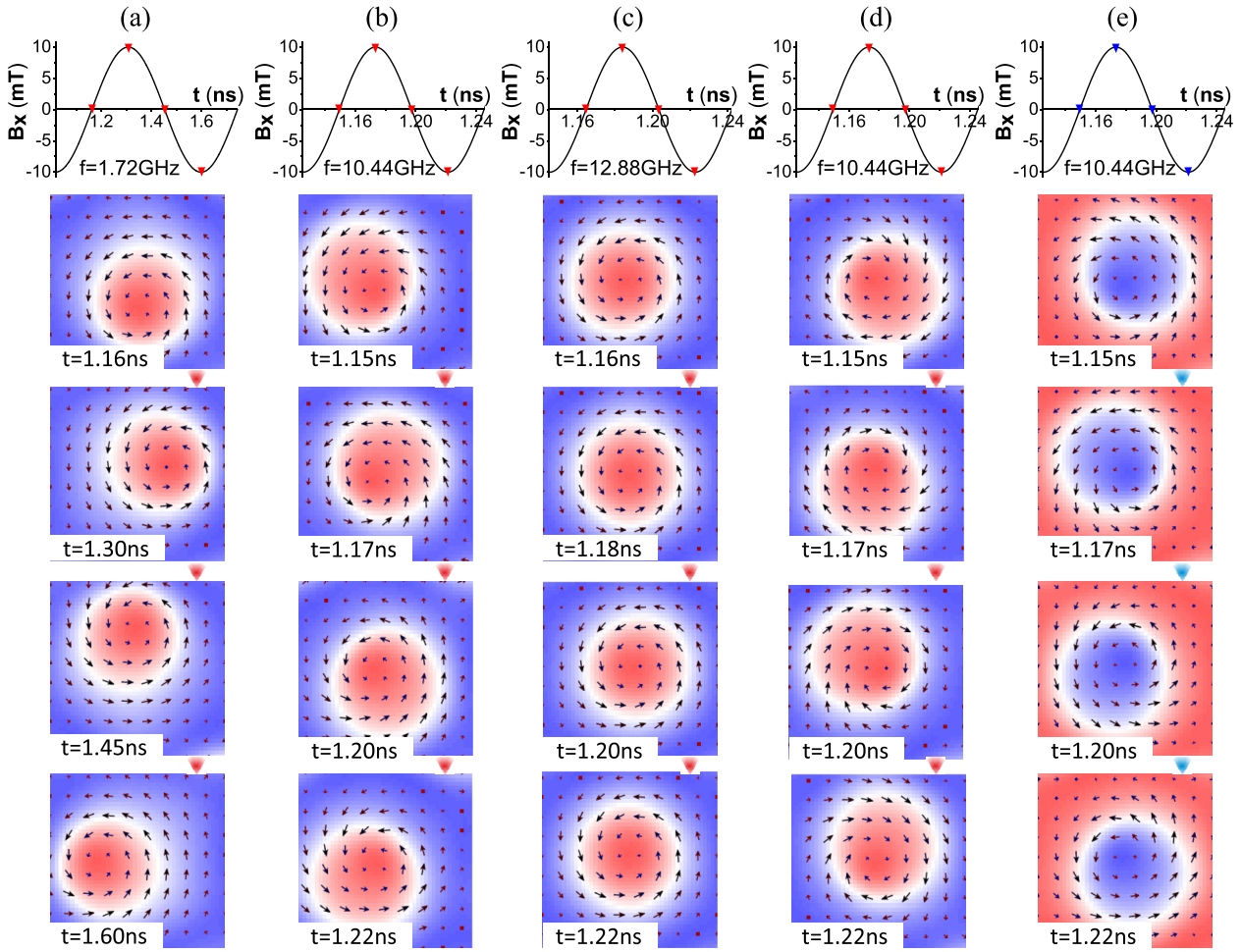

FIG. 3. Time evolution of a skyrmion core ($S = 1$) under continuous in-plane ac field at (a) 1.72 GHz, (b) 10.44 GHz, and (c) 12.88 GHz. The red/blue color denotes the magnetization coming out-of-the-surface/into-the-surface and the arrows represent the in-plane direction. (d) Time evolution of a skyrmion core ($S = 1$) under continuous in-plane ac field at 10.44 GHz similar as (b) but with opposite (CW) circulation. (e) Time evolution of a skyrmion core with $S = -1$ under a 10.44 GHz in-plane ac field.

additional resonant mode at 1.72 GHz is the gyration mode of the vortex core.

In summary, we have studied the dynamics of artificial skyrmion crystal with micromagnetic simulations. In the absence of DMI, we do observe the in-plane CCW and CW rotational mode and out-of-plane breathing mode of skyrmion crystal, evidencing that the nontrivial magnetic structure is the intrinsic origin of skyrmion dynamics. We also find the skyrmion number determines the rotation direction of in-plane mode as well as the phase of out-of-plane breathing mode, manifesting the topological nature of skyrmion dynamics.

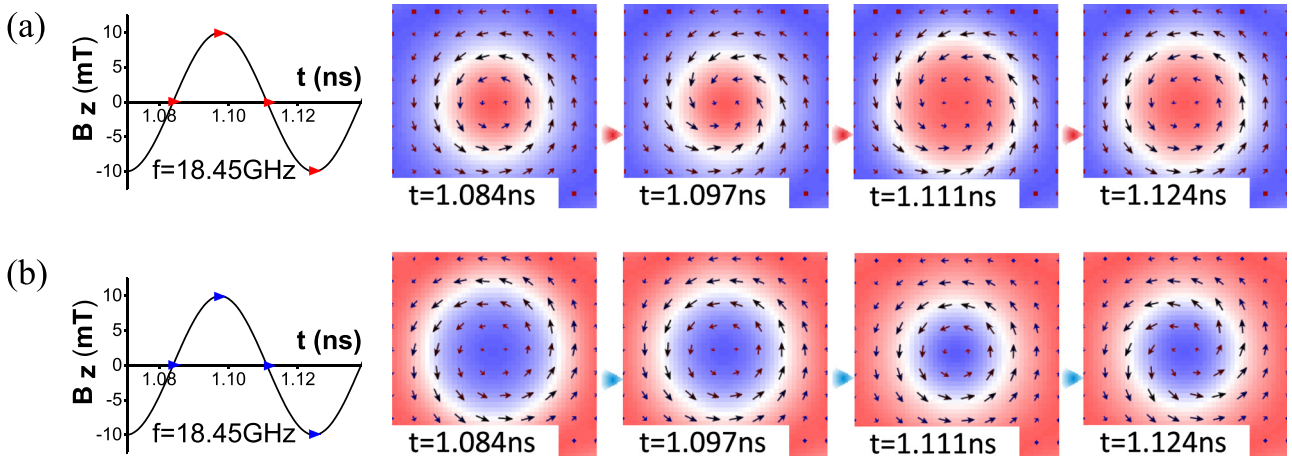

FIG. 4. Breathing mode activated by a continuous out-of-plane ac field at 18.45 GHz. The skyrmion core extends and shrinks as a function of time. Skyrmion states (a) with $S = 1$ and (b) $S = -1$ breath out-of-phase with each other.

This work was supported by the National Natural Science Foundation of China (Grant Nos. 11374145, 11304150, 11374203, and 51571109), Natural Science Foundation of Jiangsu Province (Grant No. BK20150565).

[1]S. Mühlbauer, B. Binz, F. Jonietz, C. Pfleiderer, A. Rosch, A. Neubauer, R. Georgii, and P. Böni, Science **323**, 915 (2009).
[2]X. Z. Yu, Y. Onose, N. Kanazawa, J. H. Park, J. H. Han, Y. Matsui, N. Nagaosa, and Y. Tokura, Nature **465**, 901 (2010).
[3]X. Z. Yu, N. Kanazawa, W. Z. Zhang, T. Nagai, T. Hara, K. Kimoto, Y. Matsui, Y. Onose, and Y. Tokura, Nat. Commun. **3**, 988 (2012).
[4]F. Jonietz, S. Mühlbauer, C. Pfleiderer, A. Neubauer, W. Münzer, A. Bauer, T. Adams, R. Georgii, P. Böni, R. A. Duine, K. Everschor, M. Garst, and A. Rosch, Science **330**, 1648 (2010).
[5]A. Neubauer, C. Pfleiderer, B. Binz, A. Rosch, R. Ritz, P. G. Niklowitz, and P. Böni, Phys. Rev. Lett. **102**, 186602 (2009).
[6]A. Fert, V. Cros, and J. Sampaio, Nat. Nano **8**, 152 (2013).
[7]A. Rosch, Nat. Nano **8**, 160 (2013).
[8]X. Zhang, G. P. Zhao, H. Fangohr, J. P. Liu, W. X. Xia, J. Xia, and F. J. Morvan, Sci. Rep. **5**, 7643 (2015).
[9]S.-Z. Lin, C. Reichhardt, and A. Saxena, Appl. Phys. Lett. **102**, 222405 (2013).
[10]B. Zhang, W. Wang, M. Beg, H. Fangohr, and W. Kuch, Appl. Phys. Lett. **106**, 102401 (2015).
[11]M. Mochizuki and Y. Watanabe, Appl. Phys. Lett. **107**, 082409 (2015).
[12]Y. Li, N. Kanazawa, X. Z. Yu, A. Tsukazaki, M. Kawasaki, M. Ichikawa, X. F. Jin, F. Kagawa, and Y. Tokura, Phys. Rev. Lett. **110**, 117202 (2013).
[13]U. K. Roszler, A. N. Bogdanov, and C. Pfleiderer, Nature **442**, 797 (2006).
[14]W. Münzer, A. Neubauer, T. Adams, S. Mühlbauer, C. Franz, F. Jonietz, R. Georgii, P. Böni, B. Pedersen, M. Schmidt, A. Rosch, and C. Pfleiderer, Phys. Rev. B **81**, 041203 (2010).
[15]X. Z. Yu, N. Kanazawa, Y. Onose, K. Kimoto, W. Z. Zhang, S. Ishiwata, Y. Matsui, and Y. Tokura, Nat. Mater. **10**, 106 (2011).
[16]S. X. Huang and C. L. Chien, Phys. Rev. Lett. **108**, 267201 (2012).
[17]Y. Tokunaga, X. Z. Yu, J. S. White, H. M. Ronnow, D. Morikawa, Y. Taguchi, and Y. Tokura, Nat. Commun. **6**, 7638 (2015).
[18]G. Chen, A. Mascaraque, A. T. Diaye, and A. K. Schmid, Appl. Phys. Lett. **106**, 242404 (2015).
[19]W. Jiang, P. Upadhyaya, W. Zhang, G. Yu, M. B. Jungfleisch, F. Y. Fradin, J. E. Pearson, Y. Tserkovnyak, K. L. Wang, O. Heinonen, S. G. E. te Velthuis, and A. Hoffmann, Science **349**, 283 (2015).
[20]L. Sun, R. X. Cao, B. F. Miao, Z. Feng, B. You, D. Wu, W. Zhang, A. Hu, and H. F. Ding, Phys. Rev. Lett. **110**, 167201 (2013).
[21]Y. Y. Dai, H. Wang, P. Tao, T. Yang, W. J. Ren, and Z. D. Zhang, Phys. Rev. B **88**, 054403 (2013).
[22]B. F. Miao, L. Sun, Y. W. Wu, X. D. Tao, X. Xiong, Y. Wen, R. X. Cao, P. Wang, D. Wu, Q. F. Zhan, B. You, J. Du, R. W. Li, and H. F. Ding, Phys. Rev. B **90**, 174411 (2014).
[23]J. Li, A. Tan, K. W. Moon, A. Doran, M. A. Marcus, A. T. Young, E. Arenholz, S. Ma, R. F. Yang, C. Hwang, and Z. Q. Qiu, Nat. Commun. **5**, 4704 (2014).
[24]D. A. Gilbert, B. B. Maranville, A. L. Balk, B. J. Kirby, P. Fischer, D. T. Pierce, J. Unguris, J. A. Borchers, and K. Liu, Nat. Commun. **6**, 8462 (2015).
[25]N. Nagaosa and Y. Tokura, Nat. Nano **8**, 899 (2013).
[26]A. Bauer, M. Garst, and C. Pfleiderer, Phys. Rev. Lett. **110**, 177207 (2013).
[27]M. Mochizuki, Phys. Rev. Lett. **108**, 017601 (2012).
[28]Y. Onose, Y. Okamura, S. Seki, S. Ishiwata, and Y. Tokura, Phys. Rev. Lett. **109**, 037603 (2012).
[29]Y. Okamura, F. Kagawa, M. Mochizuki, M. Kubota, S. Seki, S. Ishiwata, M. Kawasaki, Y. Onose, and Y. Tokura, Nat. Commun. **4**, 2391 (2013).
[30]F. Büttner, C. Moutafis, M. Schneider, B. Krüger, C. M. Günther, J. Geilhufe, C. v. K. Schmising, J. Mohanty, B. Pfau, S. Schaffert, A. Bisig, M. Foerster, T. Schulz, C. A. F. Vaz, J. H. Franken, H. J. M. Swagten, M. Kläui, and S. Eisebitt, Nat. Phys. **11**, 225 (2015).
[31]M. J. Donahue and D. G. Porter, *OOMMF User's Guide Version 1.0*. (National Institute of Standards and Technology, Gaithersburg, MD, 1999).
[32]M. Maret, M. C. Cadeville, R. Poinsot, A. Herr, E. Beaurepaire, and C. Monier, J. Magn. Magn. Mater. **166**, 45 (1997).
[33]C. Eyrich, W. Huttema, M. Arora, E. Montoya, F. Rashidi, C. Burrowes, B. Kardasz, E. Girt, B. Heinrich, O. N. Mryasov, M. From, and O. Karis, J. App. Phys. **111**, 07C919 (2012).
[34]R. P. Cowburn, D. K. Koltsov, A. O. Adeyeye, M. E. Welland, and D. M. Tricker, Phys. Rev. Lett. **83**, 1042 (1999).
[35]H. F. Ding, A. K. Schmid, D. Li, K. Y. Guslienko, and S. D. Bader, Phys. Rev. Lett. **94**, 157202 (2005).
[36]C. L. Chien, F. Q. Zhu, and J.-G. Zhu, Phys. Today **60**(6), 40 (2007).
[37]O. A. Tretiakov and O. Tchernyshyov, Phys. Rev. B **75**, 012408 (2007).
[38]X. Zhu, Z. Liu, V. Metlushko, P. Grütter, and M. R. Freeman, Phys. Rev. B **71**, 180408 (2005).
[39]V. Novosad, M. Grimsditch, K. Y. Guslienko, P. Vavassori, Y. Otani, and S. D. Bader, Phys. Rev. B **66**, 052407 (2002).
[40]M. Yan, G. Leaf, H. Kaper, R. Camley, and M. Grimsditch, Phys. Rev. B **73**, 014425 (2006).
[41]M. Buess, R. Höllinger, T. Haug, K. Perzlmaier, U. Krey, D. Pescia, M. R. Scheinfein, D. Weiss, and C. H. Back, Phys. Rev. Lett. **93**, 077207 (2004).
[42]M. Buess, T. P. J. Knowles, R. Höllinger, T. Haug, U. Krey, D. Weiss, D. Pescia, M. R. Scheinfein, and C. H. Back, Phys. Rev. B **71**, 104415 (2005).
[43]C. E. Zaspel, B. A. Ivanov, J. P. Park, and P. A. Crowell, Phys. Rev. B **72**, 024427 (2005).
[44]J. P. Park and P. A. Crowell, Phys. Rev. Lett. **95**, 167201 (2005).